Journal of Molecular Spectroscopy 369 (2020) 111258

Contents lists available at ScienceDirect

Journal of Molecular Spectroscopy

journal homepage: www.elsevier.com/locate/jms

Resonance enhanced two-photon ionization and mass analyzed threshold ionization spectroscopy of 4-ethylanisole

Jiayu Hao [a], Chunyang Duan [a], Yonggang Yang [a,b], Changyong Li [a,b,*], Suotang Jia [a,b]

[a] State Key Laboratory of Quantum Optics and Quantum Optic Devices, Institute of Laser Spectroscopy, Shanxi University, Taiyuan, Shanxi 030006, China
[b] Collaborative Innovation Center of Extreme Optics, Shanxi University, Taiyuan, Shanxi 030006, China

ARTICLE INFO

Article history:
Received 11 November 2019
In revised form 16 February 2020
Accepted 19 February 2020
Available online 21 February 2020

Keywords:
4-ethylanisole
Resonance enhanced two-photon ionization
Mass analyzed threshold ionization
Franck-Condon simulation
Cationic vibronic spectra

ABSTRACT

We report the resonance enhanced two-photon ionization (REMPI) and mass analyzed threshold ionization (MATI) spectra of 4-ethylanisole. The band origin of $S_1 \leftarrow S_0$ transition and accurate adiabatic ionization energy of 4-ethylanisole are determined to be 35575 ± 2 cm^{-1} and 63718 ± 5 cm^{-1}, respectively. The Franck-Condon simulation of the vibrationally resolved electronic spectrum for $D_0 \leftarrow S_1$ transition is calculated and employed to assist us in assigning the observed vibronic bands in MATI experiment. Many vibrations in the S_1 and D_0 states, not only the aromatic ring bending, OCH_3 and ethyl group bending but also their combination, are observed. The substitution effects of ethyl on transition energy and ionization energy are discussed.

1. Introduction

The aromatic ether compounds are widely applied in the fields of biology research, medicine and pesticide production, chemical synthesis and environmental protection. Ion spectroscopy is an important means to provide detailed information about the ionic properties of molecules [1]. Particularly, mass analyzed threshold ionization (MATI) spectroscopy can not only give precise ionization energy (IE) and cationic spectra of selected molecule but also has the mass-analyzed function [2,3]. Many derivatives of anisole have been studied by MATI and resonance enhanced multiphoton ionization (REMPI) spectroscopy. Eisenhardt et al. studied the high resolution spectrum of the $S_1 \leftarrow S_0$ transition of anisole [4]; Ferres et al. measured the microwave spectrum of o-methyl anisole to investigate methyl internal rotation [5]; Gellini et al. reported high overtones of the C—H stretching vibrations in anisole and thioanisole [6]; The Tzeng group investigated the vibrational features of the electronic excited state and cationic ground state of anisole and a lot of its derivatives by REMPI and MATI spectroscopy [7–16]. Mazzoni et al. reported REMPI and MATI spectra of anisole–Ar_n (n = 1, 2, 3) complexes [17]. To the best of our knowledge, the detailed spectroscopic data in the electronic excited state S_1 and cationic ground state D_0 of 4-ethylanisole are not yet available in the literature. In order to investigate the vibronic features of 4-ethylanisole in the excited state and cationic ground state, and further study the substitution effects of ethyl group on transition energy and ionization energy, we measured the REMPI, photoionization efficiency (PIE), and MATI spectra of 4-ethylanisole. A lot of vibrational bands in the electronic excited state and cationic ground state were found and assigned. We also performed density function theory (DFT) calculations and Franck-Condon simulation to help us analyze the experimental findings. The molecular structures of 4-ethylanisole in the electronic ground state S_0, excited state S_1, and cationic ground state D_0 were discussed in detail.

2. Experiments and computational details

2.1. Experimental method

The experiments were performed with two tunable UV lasers and a linear time-of-flight mass spectrometer described elsewhere [16,18,19]. The sample of liquid 4-ethylanisole (98% purity) was purchased from Macklin and used without further purification. At room temperature the liquid sample produces sufficient vapor pressure for present experiments. In order to generate the supersonic molecular beam, the sample vapors were seeded in 2 bar of krypton and expended into the vacuum chamber through a pulsed valve with a nozzle orifice of 0.8 mm in diameter. The working pressures were ~4.5×10^{-4} Pa in beam source and ~3.0×10^{-5} Pa in ionization house. After passing through a 1 mm diameter skimmer, the molecular beam was crossed with the laser beams in the ionization

* Corresponding author at: State Key Laboratory of Quantum Optics and Quantum Optic Devices, Institute of Laser Spectroscopy, Shanxi University, Taiyuan, Shanxi 030006, China.
E-mail address: lichyong@sxu.edu.cn (C. Li).

https://doi.org/10.1016/j.jms.2020.111258
0022-2852/

region. The ion field-free flight distance was ~48 cm. A dual-stacked microchannel plate (Shanxi Changcheng Microlight Equipment Co, 25 mm diameter) was used to detect the ion signal.

The experiments were initiated by utilizing two independent tunable UV laser systems whose pulse sequences were controlled by a pulse delay generator (DG645 with 8 delay outputs). The one-color (1 + 1) REMPI spectrum was measured by scanning the laser in the 273–282 nm range. The absolute wavelengths of two dye lasers were calibrated by a wavemeter (HighFinesse WS-7).

In the two-color MATI experiments, molecules were excited to long-lived high *n* Rydberg states by the two tunable UV lasers. About 100 ns after the laser pulses, a pulsed electric field of −0.7 V/cm was switched on to reject the prompt ions. After a time delay of 21 μs, a second pulsed electric field of +143 V/cm (duration = 50 μs) was applied to field-ionize the Rydberg neutrals. The mass spectra were collected and analyzed by a multichannel scaler (Stanford Research Systems, SR430), then transferred to a computer. Each mass spectrum was accumulated for 300 laser shots.

2.2. Computational method

All the geometry optimizations and frequency calculations of 4-ethylanisole were performed using the GAUSSIAN 09 program package [20]. For the first electronically excited state S_1, the time-dependent density functional theory (TD DFT) with the B3LYP functional was employed. Whereas, for the neutral ground state S_0 and the cationic ground state D_0, the density functional theory (DFT) with the B3LYP functional was used. The 6-311++G (d,p) basis set was utilized for all computations. We also performed CBS-QB3 calculations for S_0 and D_0 states to estimate the ionization energy [16]. Since the frequency calculations are on the basis of the harmonic oscillator model, the obtained frequencies are scaled by an appropriate value (0.9794 for S_1 state, and 0.9908 for D_0 state) to correct approximately for the combined errors stemming from basis set incompleteness, neglecting of electron correlation and vibrational anharmonicity.

3. Results

3.1. Molecular structure

The calculated molecular structures in S_0, S_1, and D_0 states are shown in Fig. 1. In S_0 state, just one stable structure was found. For S_1 and D_0 states, two and three stable structures were found, respectively, and we name them as S_1 *gauche-A*, S_1 *gauche-B*, D_0 *gauche*, D_0 *cis* and D_0 *trans*. In all stable structures, the OCH_3 group is in or almost in the ring-plane. In the S_0 state the substituted group C_2H_5 is out of the ring-plane and the DFT calculated value of the dihedral angle ∠6,1,11,14 is 93 degrees. For the two stable conformers of *gauche-A* and *gauche-B* in the excited state S_1, the calculated values of the dihedral angle ∠6,1,11,14 are about 62 degrees and 120 degrees, respectively. The conformers for cation of 4-ethylanisole include three stable structures, D_0 *gauche*, D_0 *cis*, and D_0 *trans* as shown in Fig. 1. For D_0 *cis* and D_0 *trans* configurations, the ethyl groups are in the ring-plane with opposite orientations. In the S_0 and D_0 *gauche* states, the group C_2H_5 is almost perpendicular to the ring-plane. In order to determine which state is probably involved in our experiment, we calculated the one-dimension potential energy surface (PES) by scanning the dihedral angle of ∠6,1,11,14, and the results are shown in Fig. 2a–c for the S_0, S_1, and D_0 state, respectively. The PES of S_0 shows that there is only one stable conformer existing in the supersonic beam. Although the calculated result for excited state S_1 shows two stable conformers, the barrier of *gauche-B* transforming to *gauche-A* just be 0.000049 hartree or 11 cm^{-1}. This means that the *gauche-B* in S_1 state is weakly bound, and its lifetime is short. If it could be observed in the experiment, its linewidth would be obviously wider than others. We did not find any broad linewidth bands in the REMPI spectrum, which means S_1 *gauche-B* conformer did not exist in our experiment. In D_0 state, although the *cis* and *trans* configurations are also stable, the Franck-Condon factors between S_1 and D_0 states are very small due to the obvious structure differences. So just one conformer, i.e. the *gauche* conformer, could exist and be observed in present experiments.

3.2. REMPI spectrum of 4-ethylanisole

Fig. 3 shows the REMPI spectrum of 4-ethylanisole in the energy range near its $S_1 \leftarrow S_0$ electronic transition. The pronounced band located at 35575 cm^{-1} is identified as the origin of $S_1 \leftarrow S_0$ transition. 4-ethylanisole has 60 normal vibrational modes, including 18 ethyl, 30 benzene-like and 12 methoxyl vibronic modes. For benzene derivatives, the $S_1 \leftarrow S_0$ transition is mainly subject to the $\pi^* \leftarrow \pi$ electronic excitation, leading to an expansion in the ring. This gives rise to many active vibronic transitions related to the benzene-like vibrations. Only the vibronic transitions with lager Franck-Condon factor can be observed in the REMPI spectrum [21,22]. The experimental and calculated vibration frequencies of 4-ethylanisole in S_1 state are listed in Table 1. The assignments

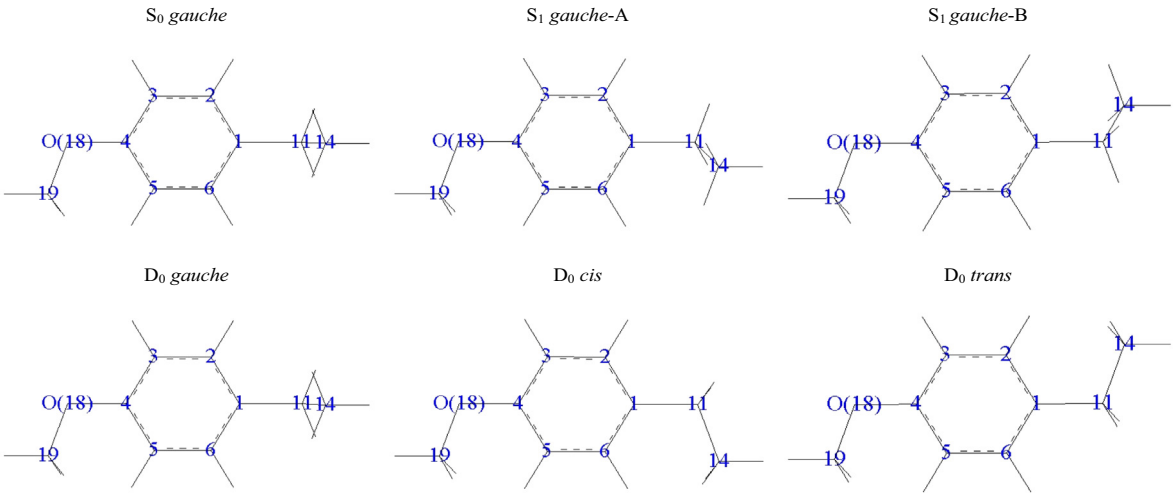

Fig. 1. Theoretically calculated stable structures of the neutral ground state S_0, electronic excited state S_1, and cationic ground state D_0 of 4-ethylanisole. For details on the structure, see Section 3.1.

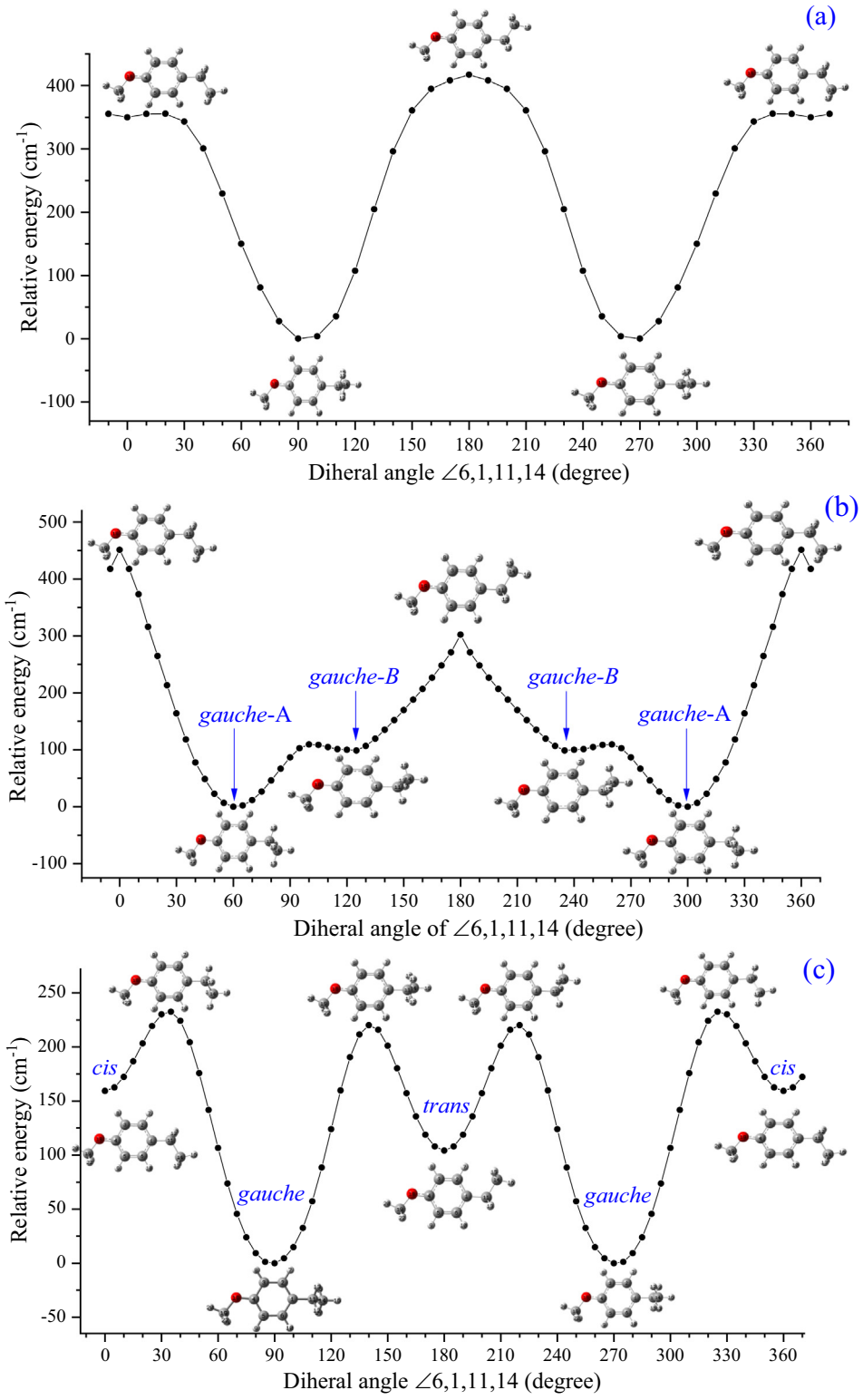

Fig. 2. The potential curves of (a) S_0, (b) S_1, and (c) D_0 state calculated by scanning the dihedral angle ∠6,1,11,14 at the level of B3LYP/6311G++(d,p), TD-B3LYP/6311G++(d,p), and B3LYP/6311G++(d,p), respectively.

are based on our TD-DFT calculation at B3LYP/6-311++G (d,p) level and previous publications on 4-methylanisol [13] and 4-methylphenol [23]. The labeling convention of the vibrational modes follows the Varsanyi's system [24], which is based on the Wilson's notation [25]. The weak bands at 63, 299, 487, 605, 676, and 728 cm^{-1} are assigned to the transitions of 11^1_0, $10b^1_0$, $10a^1_0$, 4^1_0, $17b^1_0$, and 5^1_0, respectively. These bands belong to out-of-plane bending of the ring. The pronounced bands at 397, and 498, 553 cm^{-1} correspond to transitions $9b^1_0$, $6a^1_0$, and $6b^1_0$, respectively, which belong to in-plane bending of the ring. And the band at 790 cm^{-1} is assigned to the ring breathing vibration 1^1_0. The weak

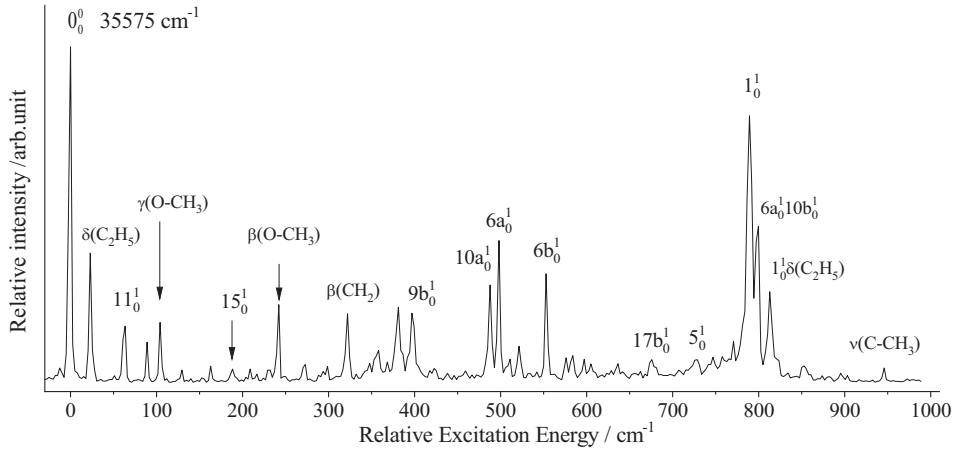

Fig. 3. REMPI spectrum of 4-ethylanisole. The spectrum is shifted by 35575 cm^{-1}. The laser energy was maintained at about 6 μJ when scanning wavelength of the dye laser.

Table 1
Vibrational frequencies (in cm^{-1}) and assignments of observed bands in the REMPI spectrum of 4-ethylanisole.[a]

This work Exp. [a]	Exp.Rel. Int.	Cal.	Assignment[b]
0	100		0_0^0, band origin
23	38	41	δ(C$_2$H$_5$), C$_2$H$_5$ torsion
63	17	60	11_0^1,γ(CCC)
89	12		$11_0^1\delta(C_2H_5)$
104	18	110	γ(O-CH$_3$)
130	4		11_0^2
163	5		$11_0^1\gamma$(O-CH$_3$)
188	4	187	15_0^1, β(O-CH$_3$), β(C-C$_2$H$_5$)
209	4	208	τ(CH$_3$)
242	23	248	β(O-CH$_3$)
273	5		$11_0^1\tau$(CH$_3$)
299	5	302	$10b_0^1$, γ(CCC)
322	20	339	β(CH$_2$)
358	9		β(O-CH$_3$)
381	22		$11_0^1\beta$(CH$_2$)
397	21	408	$9b_0^1$, β(O-CH$_3$), β(C- C$_2$H$_5$)
487	29	466	$10a_0^1$, γ(CH)
498	42	494	$6a_0^1$, β(CCC)
521	11		$6a_0^1$ δ(C$_2$H$_5$)
553	32	563	$6b_0^1$, β(CCC)
576	7		$6b_0^1$ δ(C$_2$H$_5$)
584	8		$6a_0^1 11_0^1$ δ(C$_2$H$_5$)
597	7		$10b_0^2$
605	5	604	4_0^1, γ(CCC)
636	6		$6b_0^1 11_0^1$ δ(C$_2$H$_5$)
676	7	672	$17b_0^1$, γ(CH)
728	7	723	5_0^1, γ(CCC)
790	80	792	1_0^1, breathing
799	46		$6a_0^1 10b_0^1$
813	27		1_0^1 δ(C$_2$H$_5$)
853	5		$1_0^1 11_0^1$
946	4	937	ν(C-CH$_3$)

[a] The experimental values are shifts from 35575 cm^{-1}, whereas the calculated ones are obtained from the TD-B3LYP/6-311G++(d,p) calculation, scaled by 0.9794.
[b] ν, stretching; β, in-plane bending; γ, out-of-plane bending; τ, CH$_3$ internal rotation; δ, C$_2$H$_5$ torsion.

bands at 188 cm^{-1} is assigned to the transitions of 15_0^1, which belong to in-plane bending of the ring. The vibrational modes of substituents are also observed. The ethyl torsion δ(C$_2$H$_5$) is located at 23 cm^{-1}, and the in-plane bending of CH$_2$ β(CH$_2$) is located to 322 cm^{-1}. The bands at 104 and 242 cm^{-1} result from the out-of-plane bending of methoxy γ(O-CH$_3$) and in-plane bending of methoxy β(O-CH$_3$). The bands at 358, 597, and 799 cm^{-1} are related to the combination vibration $11_0^2\beta$(O-CH$_3$), overtone vibration $10b_0^2$, and combination vibration $6a_0^1 10b_0^1$, respectively. Other bands observed in the Fig. 1 are assigned to the substituent vibrations or the combinations of several vibrational modes as listed in Table 1.

3.3. PIE spectrum of 4-ethylanisole

The photoionization efficiency (PIE) spectrum is easily obtained due to the intense probe signal. So we first measured the PIE curve of 4-ethylanisole before the MATI experiment. Fig. 4 shows the PIE curve recorded via the $S_1 0^0$ (35575 cm^{-1}) intermediate state. Investigation on the rising step indicates the adiabatic ionization energy of 4-ethylanisole to be 63718 cm^{-1}, which was empirically estimated by taking the (1 + 1′) two-photon energy at the point of 3/4 of the rising step as the ionization energy under present experimental condition, with an uncertainty of 10 cm^{-1} [16,19,23]. The CBS-QB3 calculation yields the IE of 63455 cm^{-1}, which is just lower than the measured one by 263 cm^{-1}. And the relative errors of CBS-QB3 calculation is just −0.41% for 4-ethylanisole. This theoretical calculation helps us to select the right dye for the experimental measurement.

3.4. MATI spectra of 4-ethylanisole

Fig. 5 gives the MATI spectra of 4-ethylanisole, recorded via the 0^0, γ(O-CH$_3$), and β(O-CH$_3$) vibrational levels of the S_1 state. To our knowledge, the IE of 4-ethylanisole is not yet available in the literature. Since the MATI experiment detects the threshold ions resulting from the field ionization of the high Rydberg state molecules, it leads to a sharp peak at the ionization limit. In this way, it yields a more precise IE than the PIE technique. And the energy shift due to the Stark effect of the pulsed electronic field may be approximated to be $4.0F^{1/2}$ (F = 0.5 V/cm in present experiments) [16,23]. Analysis of the most intense band 0^+ in Fig. 5a generates the adiabatic IE of 63718 ± 5 cm^{-1}, which is in excellent agreement with PIE measured value.

Table 2 lists the observed vibrational frequencies of 4-ethylanisole in the D_0 state, along with the corresponding calculated frequencies and their possible assignments. And the spectral assignment was mainly based on the B3LYP/6-311++G(d,p) calculations, Franck-Condon simulation, and previous publications

[13,23]. As shown in Fig. 5(a), when the level $S_1 0^0$ is used as the intermediate state, the pronounced band at 805 and 1627 cm^{-1} are assigned to ring breathing vibration 1^1 and the in-plane stretching vibrations $8a^1$, respectively. The bands at 421, 513, and 1223 cm^{-1} result from the in-plane aromatic ring deformation vibrations $9b^1$, $6a^1$, and 13^1 of 4-ethylanisole cation, respectively. The weak bands at 71, 330, and 371 cm^{-1} correspond to the out-of-plane deformation vibration 11^1, $10b^1$, and $16a^1$, respectively. Other bands are assigned to vibrations of substituent methoxy and ethyl or combinations of several modes. Fig. 5(b) shows the MATI spectrum recorded via the $\gamma(O\text{-}CH_3)$ of the S_1 state. The $\Delta v = 0$ propensity rule is well observed [18,19,26]. The methoxy vibration $\gamma(O\text{-}CH_3)$ is the most intense. The combination band of breathing vibration with $\gamma(O\text{-}CH_3)$ is the second most intense. Except for 166 and 973 cm^{-1} belonging to rotation of methyl group of OCH_3 $\tau(CH_3)$ and combination vibration $1^1\tau(CH_3)$, respectively, other most bands can be assigned to combination of $\gamma(O\text{-}CH_3)$ with those bands observed in Fig. 5(a). Similar to the Fig. 5(b), when the $S_1\beta(O\text{-}CH_3)$ is used as the intermediate state, the vibration pattern of the most intense band in the MATI spectrum is the same as the intermediate state, i.e. assigned as $\beta(O\text{-}CH_3)$ as shown in the Fig. 5 (c). Except for bands at 253, 285, and 561 cm^{-1} are assigned to $\delta(C_2H_5)\gamma(C\text{-}OCH_3)$, $\gamma(O\text{-}CH_3)^2$, and $16b^1$ vibrations, other bands are assigned as combinations of $\beta(O\text{-}CH_3)$ with observed bands in Fig. 5(a). All measured MATI bands together with the calculated frequencies and their possible assignments and approximate descriptions are listed in Table 2. We also attempt to measure the MATI spectrum via $S_1 1^1$ intermediate state, but the signal-to-noise rate is very small, and the result could not provide more information on the D_0 state.

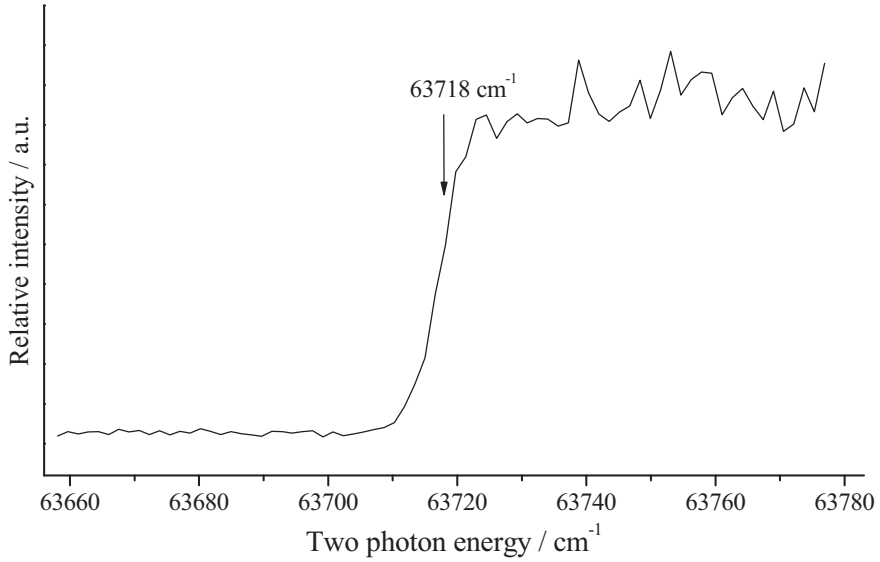

Fig. 4. Photoionization efficiency curve of 4-ethylanisole via the $S_1 0^0$ intermediate state.

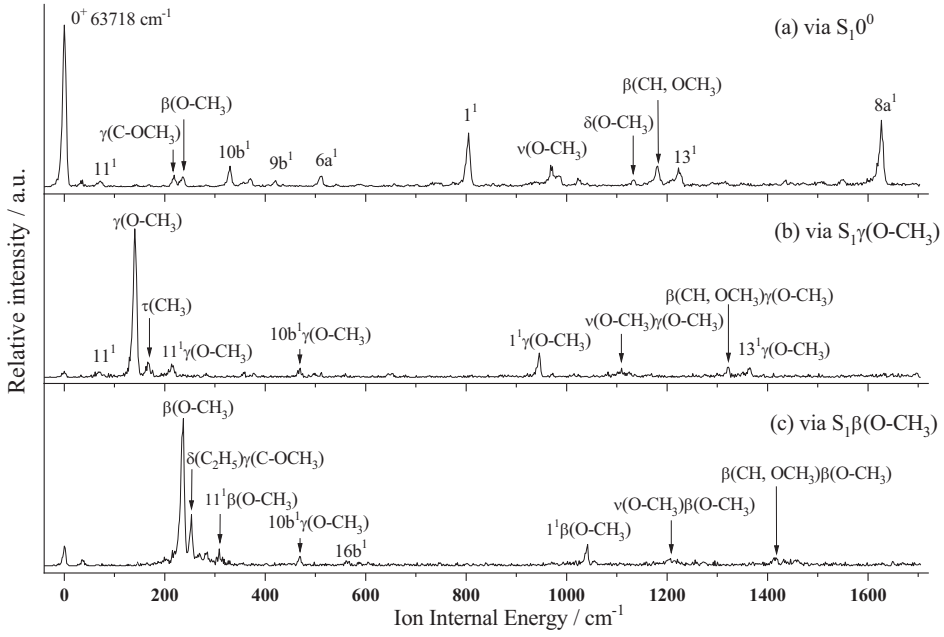

Fig. 5. MATI spectra of 4-ethylanisole recorded via (a) $S_1 0^0$, (b) $S_1\gamma(O\text{-}CH_3)$, and (c) $S_1\beta(O\text{-}CH_3)$.

4. Discussion

4.1. MATI spectrum simulation

In order to give the right spectral assignment, the spectrum simulation is usually needed. The structural similarity between the two electronic states involved in electronic transitions is important for spectral simulation. In Section 3.1 we show the calculated results on molecular structures in S_0, S_1, and D_0 states. The structure (mainly the ethyl orientation) in S_1 state is very different from the S_0 and D_0 states, which makes the Frank-Condon factor approximately equal to zero, and result in failure of the spectral simulations of REMPI and MATI. This suggests that current theoretical calculations on molecular structure may involve large errors. We attempt to freeze the orientation of ethyl to a lot of different degrees with respect to the ring-plane to perform the structural optimization and frequency calculation for the S_1 state. The results show that when the dihedral angle ∠6,1,11,14 is frozen to a value in the range of 60 to 79.5 degree, no negative frequency appear in results; while when it is greater than 80 degree and less than 108 degree, a negative frequency always appear in the result. Although in the former case no negative frequency appear in the result, the spectral simulation is also unsuccessful. At last we change the ethyl orientation to the same as the stable S_1 *gauche*-A state, and froze dihedral angle ∠6,1,11,14 to perform the geometry optimization and frequency calculation for the S_0 and D_0 states. The calculated results do not include any negative frequency. Further Franck-Condon spectral simulations of $S_1 \leftarrow S_0$ and $D_0 \leftarrow S_1$ are successful. The detail of FC calculation can be found in Ref. [27]. Here we show the simulation of $D_0 \leftarrow S_1$ transition together with the measured MATI spectrum in Fig. 6 as a comparison. The calculated result, in particular the vibrational frequencies, is in good agreement with the measured MATI. For the vibrational bands of $8a^1$, 13^1, β(CH) and ν(O-CH_3), both the frequencies and the intensity are in good agreement between the calculated and measured results. The $16a^2$ band is so weak in measured MATI spectrum that we might ignore it if we could not simulate the spectrum of $D_0 \leftarrow S_1$ well. It indicates that the FC simulation is important for the spectral assignment.

4.2. Para-substitution effect on the transition energy and ionization energy of anisole

For benzene derivatives, the substituent can interact with the aromatic ring by conjugation (resonance) effect through the π orbital and inductive effect through σ bond. The collective effect can cause a slight change on the nearby electron density and the molecular geometry, and results in a small extent of reduction in the zero-point energy (ZPE) level of electronic state. If the degree of the reduction in the ZPE level of the upper electronic state is greater than that in the lower one, it leads to a red shift in the transition energy. Conversely, it yields a blue shift [28].

Table 2
Vibrational frequencies (in cm^{-1}) and assignments of observed bands in the MATI spectra of 4-ethylanisole.[a]

Intermediate level in the S_1 state				
0^0	γ(O-CH_3)	β(O-CH_3)	Cal.	Assignment[b]
36			33	δ(C_2H_5)
71	71		66	11^1, γ(CCC)
	141		140	γ(O-CH_3)
	166		150	τ(CH_3), at OCH_3
	176			γ(O-CH_3) δ(C_2H_5)
	214			11^1γ(O-CH_3)
219			218	γ(C-OCH_3)
236		237	233	β(O-CH_3)
		253		γ(C-OCH_3) δ(C_2H_5)
	283	285		γ(O-CH_3)^2
		309		11^1β(O-CH_3)
330			329	$10b^1$, γ(CCC)
371			377	$16a^1$, γ(CCC)
	378			γ(O-CH_3) β(O-CH_3)
421			420	$9b^1$, β(CCC)
	470	469		γ(O-CH_3)$10b^1$
	512			γ(O-CH_3)$16a^1$
513			511	$6a^1$, β(CCC)
		561	548	$16b^1$, γ(CH)
741				$16a^2$
805			805	1^1, breathing
	946			1^1γ(O-CH_3)
968			966	ν(O-CH_3)
	973			1^1τ(CH_3)
1023			1023	β(C_2H_5)
		1042		1^1β(O-CH_3)
	1110			ν(O-CH_3)γ(O-CH_3)
1134			1139	δ(OCH_3)
1182			1182	β(CH) , at OCH_3
		1207		β(O-CH_3) ν(O-CH_3)
1223			1226	13^1, ν(C- C_2H_5)
		1256		β(O-CH_3) β(C_2H_5)
	1322			γ(O-CH_3) β(CH)
	1365			13^1 γ(O-CH_3)
		1417		β(O-CH_3)β(CH)
1437			1449	γ(CH) , at OCH_3
1551				$1^1 16a^2$
		1457		13^1β(O-CH_3)
1627			1641	$8a^1$, ν(CCC)

[a] The experimental values are shifts from 63718 cm^{-1}, whereas the predicted ones are obtained from the B3LYP/6311G++(d,p) calculations, scaled by 0.9908.
[b] ν, stretching; β, in-plane bending; γ, out-of-plane bending; τ, CH_3 internal rotation; δ, torsion.

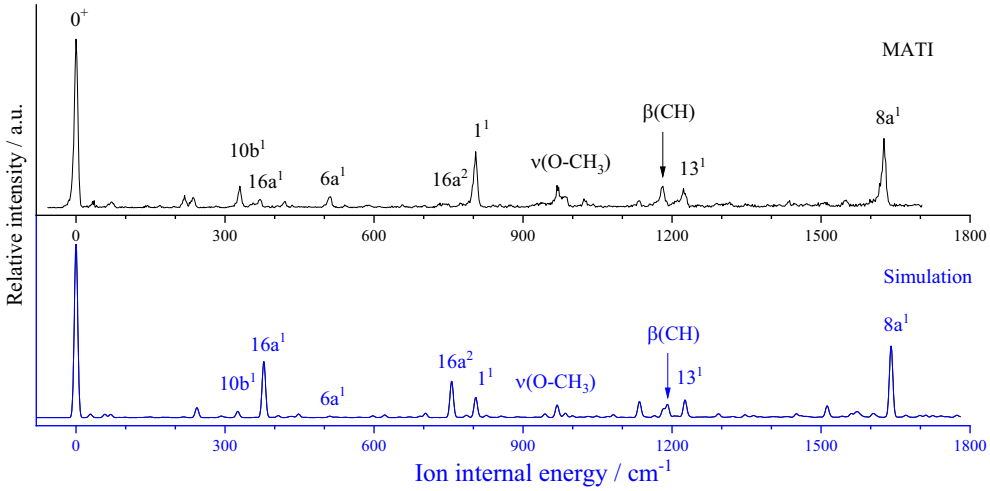

Fig. 6. MATI spectrum of 4-ethylanisole recorded via the $S_1 0^0$ intermediate state and its Franck-Condon simulation.

Table 3
Measured electronic transition and inoization energies (cm^{-1}) of anisole and it derivatives.[a]

Molecule	Substituent formula	$E_1(S_1 \leftarrow S_0)$	ΔE_1	$E_2(D_0 \leftarrow S_1)$	ΔE_2	IE	ΔIE	Ref.
Anisole		36,383	0	30,016	0	66,399	0	[7]
4-aminoanisole	NH_2	31,581	−4802	25,864	−4152	57,445	−8954	[8]
trans-p-dimethoxybenzene	OCH_3	33,631	−2752	26,932	−3084	60,563	−5836	[9,10]
cis-p-dimethoxybenzene	OCH_3	33,852	−2531	26,920	−3096	60,772	−5627	[9,10]
4-methoxyphenol trans	OH	33,572	−2811	28,638	−1378	62,210	−4189	[11]
4-methoxyphenol cis	OH	33,667	−2716	28,646	−1370	62,313	−4086	[11]
cis-p-methoxystyrene	CH_2CH	33,250	−3133	29,237	−779	62,487	−3912	[12]
trans-p-methoxystyrene	CH_2CH	33,325	−3058	29,187	−829	62,512	−3887	[12]
4-ethylanisole	C_2H_5	35,575	−808	28,141	−1875	63,718	−2683	This work
4-methylanisole	CH_3	35,410	−973	28,382	−1634	63,792	−2607	[13]
4-chloroanisole	Cl	34,861	−1522	31,251	1235	66,112	−287	[14]
4-fluoroanisole	F	35,146	−1237	31,291	1275	66,437	38	[15]
4-cyanoanisole	CN	35,549	−834	34,860	4844	70,409	4010	[16]

[a] ΔE_1, ΔE_2, and ΔIE are shitfs of E_1, E_2 and IE with respect to anisole.

Table 3 lists the measured transition energies and adiabatic ionization energies of anisole and some of its derivatives from the REMPI, ZEKE, and MATI spectroscopy [7–16]. It shows that the substitutions of NH_2, *trans-p*-OCH_3, *cis-p*-OCH_3, *trans-p*-OH, *cis-p*-OH, *cis-p*-CH_2CH, *trans-p*-CH_2CH, C_2H_5, CH_3, Cl, F, CN on the *para* position of anisole cause the excited energy $E_1(S_1 \leftarrow S_0)$ to be lowered by 4802, 2752, 2531, 2811, 2716, 3133, 3058, 808, 973, 1522, 1237, 834 cm^{-1}, respectively. This indicates that the interaction of the substituent and the ring in the upper electronic state S_1 is stronger than that in the lower state S_0. In particular, the substitutions of NH_2, OCH_3, OH, and CH_2CH cause greater red shifts than C_2H_5, CH_3, Cl, F, and CN group, indicating the greater interactions between the substituent of NH_2, OCH_3, OH, CH_2CH and the aromatic ring. The existing literatures reported that the red shift most probably result from the dominant conjugation effect upon $S_1 \leftarrow S_0$ transition [28–31].

The transition of E_2 ($D_0 \leftarrow S_1$) mainly involve removing an electron from the excited state S_1. The substitution of Cl, F, CN on the *para* position of anisole causes the transition energy E_2 to be increased by1235, 1275, 4844 cm^{-1}, respectively. This indicates that the group of Cl, F, CN enhances bond force of the anisole binding the valence electrons, and shows that Cl, F, and CN are the electron-withdrawing groups. Other substitutions cause the transition energy E_2 to be lowered by the magnitude of 779 to 4152 cm^{-1}. It shows that NH_2, OCH_3, OH, CH_2CH, C_2H_5, and CH_3 reduce bond force of the anisole binding the valence electrons, and they can be considered as the electron-donating groups.

The adiabatic ionization energy is determined by adding the transition energy $E_1(S_1 \leftarrow S_0)$ and $E_2(D_0 \leftarrow S_1)$. It is known from Table 3 that $E_1(S_1 \leftarrow S_0)$ always redshift with respective to parent molecule anisole, and E_2 ($D_0 \leftarrow S_1$) is blueshift for the electron-withdrawing groups Cl, F, and CN and redshift for the others (electron-donating groups). The collective effect makes the IE of 4-fluoroanisole and 4-cyanoanisole to be blue shift, and other molecules are red shift. From shift value we can estimate the electron-withdrawing ability order follows CN > F > Cl, and the electron-donating ability order follows $NH_2 > OCH_3 > OH > CH_2CH > C_2H_5 > CH_3$. It is notable that the values of E_1, E_2, and IE of 4-ethylanisole and 4-methylanisole are very close, which indicates that the chemical characteristics of ethyl and methyl are very similar.

5. Conclusion

We have performed the REMPI and MATI spectroscopy to study the vibrational features of 4-ethylanisole in the S_1 and D_0 states. The band origin of the $S_1 \leftarrow S_0$ electronic transition and adiabatic ionization energies of 4-ethylanisole were determined to be 35575 ± 2 cm^{-1} and 63718 ± 5 cm^{-1}, respectively. Many ring vibration modes, both in-plane bending and out-of-plane bending, were observed in the S_1 and D_0 states of 4-ethylanisole. When the vibrational mode of OCH_3 as an intermediate state, most of active vibrations of 4-ethylansiole in MATI spectra are the combinations of the OCH_3 vibration with those observed in the MATI via $S_1 0^0$ intermediate state.

The orientation of ethyl group with respect to aromatic ring is important for the Franck-Condon simulation of electronic transition $D_0 \leftarrow S_1$ and $S_1 \leftarrow S_0$. We freeze the orientation of ethyl group of S_0 and D_0 states the same as the S_1 stable state to perform the geometry optimizations and frequency calculations. Further the Franck-Condon simulation is in good agreement with our experimental result. Franck-Condon simulation assisted us in explaining experimental findings. The ethyl substitution effects on transition energy and ionization energy are close to methyl group.

CRediT authorship contribution statement

Jiayu Hao: Investigation, Writing - original draft. **Chunyang Duan:** Investigation. **Yonggang Yang:** Funding acquisition. **Changyong Li:** Project administration, Writing - review & editing. **Suotang Jia:** Conceptualization, Funding acquisition, Resources.

Declaration of Competing Interest

The authors declare that they have no known competing financial interests or personal relationships that could have appeared to influence the work reported in this paper.

Acknowledgments

This work was supported by National Key R&D Program of China (Grant No. 2017YFA0304203), National Natural Science Foundation of China (Grants Nos. 61575115, 61835007, 11434007, 61378039), PCSIRT (No. IRT_17R70), 111 project (Grant No. D18001), the Construction of State Key Laboratory of Quantum Optics and Quantum Optics Devices, China (Grant No. 2015012001-20), and the Fund for Shanxi"1331 Project" Key Subjects Construction.

References

[1] K. Müller-Dethlefs, E.W. Schlag, Angew. Chem. Int. Ed. 37 (1998) 1346–1374.
[2] L. Zhu, P. Johnson, J. Chem. Phys. 94 (1991) 5769–5771.
[3] S. Ullrich, W.D. Geppert, C.E.H. Dessent, K. Müller-Dethlefs, J. Phys. Chem. A 104 (2000) 11864.
[4] C.G. Eisenhardt, G. Pietraperzia, M. Becucci, Phys. Chem. Chem. Phys. 3 (2001) 1407–1410.
[5] L. Ferres, H. Mouhib, W. Stahl, H.V.L. Nguyen, ChemPhysChem 18 (2017) 1855–1859.
[6] C. Gellini, L. Moroni, M. Muniz-Miranda, J. Phys. Chem. A 106 (2002) 10999–11007.
[7] M. Pradhan, C. Li, J.L. Lin, W.B. Tzeng, Chem. Phys. Lett. 407 (2005) 100–104.
[8] J. Lin, J.L. Lin, Wen Bih Tzeng, Chem. Phys. Lett. 370 (2003) 44–51.
[9] W.B. Tzeng, K. Narayanan, C.Y. Hsieh, C.C. Tung, J. Mol. Struct. 448 (1998) 91–100.
[10] J.L. Lin, L.C.L. Huang, W.B. Tzeng, J. Phys. Chem. A 105 (2001) 11455–11461.
[11] C. Li, H. Su, W.B. Tzeng, Chem. Phys. Lett. 410 (2005) 99–103.
[12] C. Qin, S.Y. Tzeng, B. Zhang, W.B. Tzeng, Chem. Phys. Lett. 503 (2011) 25–28.
[13] J. Huang, C. Li, W.B. Tzeng, Chem. Phys. Lett. 414 (2005) 276–281.
[14] S.Y. Tzeng, K. Takahashi, W.B. Tzeng, Chem. Phys. Lett. 731 (2019) 136626.
[15] K.S. Shiung, D. Yu, S.Y. Tzeng, W.B. Tzeng, Chem. Phys. Lett. 524 (2012) 38–41.
[16] Y. Jin, Y. Zhao, Y. Yang, L. Wang, C. Li, S. Jia, Chem. Phys. Lett. 692 (2018) 395–401.
[17] F. Mazzoni, M. Becucci, J. Rezac, D. Nachtigallova, F. Michels, P. Hobza, K. Muller-Dethlefs, Phys. Chem. Chem. Phys. 17 (2015) 12530.
[18] Y. Zhao, Y. Jin, J. Hao, Y. Yang, L. Wang, C. Li, S. Jia, Spectrochim. Acta A 207 (2019) 328–336.
[19] Y. Zhao, Y. Jin, C. Li, S. Jia, J. Mol. Spectrosc. 363 (2019) 111182.
[20] M.J. Frisch, G.W. Trucks, H.B. Schlegel, G.E. Scuseria, M.A. Robb, et al., Gaussian 09, Revision C.01, Gaussian, Inc., Wallingford, CT, 2009.
[21] S. Schumm, M. Gerhards, K. Kleinermanns, J. Phys. Chem. A 104 (2000) 10648.
[22] J. Bloino, M. Biczysko, O. Crescenzi, V. Barone, J. Chem. Phys. 128 (2008) 244105.
[23] J.L. Lin, C. Li, W.B. Tzeng, J. Chem. Phys. 120 (2004) 10513–10519.
[24] G. Varsanyi, Assignments of Vibrational Spectra of Seven Hundred Benzene Derivatives, Wiley, New York, 1974.
[25] E.B. Wilson, Phys. Rev. 45 (1934) 706–714.
[26] C. Li, J.L. Lin, W.B. Tzeng, J. Chem. Phys. 122 (2005) 044311.
[27] J.B.V. Barone, M. Biczysko, Vibrationally-resolved electronic spectra in GAUSSIAN 09, GAUSSIAN 09, Revision A.02, 2009, available online at http://dreamsnet.sns.it/sites/default/files/download/docs/vibronic_spectra_G09-A02.pdf.
[28] Y. Zhao, Y. Jin, J. Hao, Y. Yang, C. Li, S. Jia, Chem. Phys. Lett. 711 (2018) 127–131.
[29] J. Huang, K. Huang, S. Liu, Q. Luo, W. Tzeng, J. Photochem. Photobiol. A Chem. 193 (2008) 245–253.
[30] D. Yu, C. Dong, M. Cheng, L. Hu, Y. Du, Q. Zhu, C. Zhang, J. Mol. Spectrosc. 265 (2011) 86–91.
[31] J. Huang, J.L. Lin, W.B. Tzeng, Chem. Phys. Lett. 422 (2006) 271–275.